Sensors & Transducers, Vol. 271, Issue 4, December 2025, pp. 78-85

www.sensorsportal.com

Sensors & Transducers

Published by IFSA Publishing, S. L., 2025
http://www.sensorsportal.com

A Study on a Front Illuminated GePb/GeSiPb based Barrier-well-barrier Heterostructure at High Frequency Region Using SILVACO TCAD

[1, 2] Saurav GHOSH, [3] Vedatrayee CHAKRABORTY, [4] Swagata DEY, [1, 2, *] Abhishek SAHA and [1] Rudra Sankar DHAR

[1] Department of Electronics and Communication Engineering, National Institute of Technology Mizoram, Aizawl, Mizoram 796012, India

[2] Department of ECE, Dream Institute of Technology, Kolkata-700104, India
[3] Department of ECE, B. P. Poddar Institute of Management & Technology, Kolkata-700052, India

[4] Department of Electronics, Bhairab Ganguly College, Belghoria, Kolkata-700056, India
[*] E-mail: abhishek.ece.phd@nitmz.ac.in

Received: 9 October 2025 / Revised: 2 Dec. 2025 / Accepted: 24 Dec. 2025 / Published: 30 Dec. 2025

Abstract: The GePb-based device is emerging as a significant competitor to traditional Group III-V photonic devices. Direct bandgap III-V materials employed in optoelectronic devices, including GaAs, are expensive and pose safety risks. However, a notable enhancement is achieved by alloying lead with Germanium (Ge) or silicon (Si) or their respective alloys ($Ge_{1-x}Si_x$). The SiGePb-based Barrier-Well-Barrier heterostructure, operating in the mid- to far-infrared range, has been analyzed both analytically and through simulations conducted using the Silvaco TCAD simulator. Adding lead (Pb) to Group IV heterostructures ($Ge_{1-x}Si_x$) has shown that it can change the energy levels and create quantum confinement effects. The band profile and band offsets are analysed and compared with theoretical values, concluding that the structure is a compressively strained type II model. The calculated crossover concentration of Pb for the transition from an indirect to a direct bandgap is 0.3 %. The absorption coefficient and optical gain are determined using the carrier injection method, with the peak gain compared to the corresponding experimental data.

Keywords: Energy-bands, Band-offsets, Heterostructure, Optical gain, TYPE-II.

1. Introduction

Group IV semiconductors like Silicon (Si), Germanium (Ge), and their alloys ($Ge_{1-x}Si_x$) are important for modern electronics because of their excellent electronic properties and are compatible with CMOS technology [1]. Ge has a 0.664 eV indirect bandgap at the L valleys and a 0.800 eV direct bandgap at the Γ valleys. To transfer Ge into an efficient light emitting material, the difference between the direct and the indirect bandgaps can be compensated by introducing thermally expansion tensile strain in the Ge epilayer [2]. $Ge_{1-x}Si_x$ heterostructures (CMOS compatible) take advantage of the strain engineering and bandgap tunability of the Ge-Si system. However, because of their indirect bandgap, Group IV semiconductors, including silicon (Si) and Germanium (Ge), have low light emission efficiency. Ge or Si alloyed with Sn, C, or Pb yields a significant improvement [3-5]. The alloy of C, Sn or Pb in $Ge_{1-x}Si_x$ heterostructure will make a crossover of indirect to direct bandgap. In this way the alloyed material becomes potential light emitters due to the improvement of its light emission efficiency. A new

Si-based material GePb which has been predicted to possess a direct-bandgap attracts much attention in the field of fabricating Si-based light source recently [6]. The most researched materials are combinations of Si and its alloy with Ge, called $Ge_{1-x}Si_x$, because they work well with CMOS processing and can produce light at a wavelength of 1550 nm, which is used in telecommunications [7]. Lasing action in the heterostructure can be achieved by injecting a sufficient excess of carrier concentration. $Ge_{1-x}Si_x$-based optoelectronic systems offer a vital route towards scalable and integrable silicon photonics as the need for fast, energy-efficient data transmission keeps increasing [8]. However, the alloy composition (Sn or Pb) must be precisely optimized to minimize lattice mismatch and avoid structural deformation of the semiconductor device [9-10].

However, the strain caused by the significant lattice mismatch between Si and Ge modifies the band structure [11-14]. Soref et.al. [15] examined the variations in the band gap when they added suitable Sn composition into SiGe alloys. The important prediction made by the researchers is that the direct band gap may be achieved in SiGeSn ternary alloys for some compositions of Sn and Pb. Pb incorporation into $Ge_{1-x}Si_x$-based heterostructure preferentially lowers the Γ-valley energy relative to the L-valley. By using virtual crystal approximation (VCA) combined with density functional theory (DFT) [16-17], the crossover value of Pb concentration is evaluated to be 1 %, which is much lower than that of GeSn.

Germanium–lead (GePb), a group-IV compounds recently predicted to exhibit a direct bandgap, has emerged as a material of growing interest for developing Si-compatible light sources [18]. Like GeSn, GePb undergoes an indirect-to-direct bandgap transition with increasing Pb concentration. Calculations based on the virtual crystal approximation (VCA) combined with density functional theory (DFT) predict that this transition occurs at only ~1 % Pb content—much lower than the ~11 % crossover concentration reported for GeSn using the same method [18]. This suggests that GePb could represent a more promising direct-bandgap alloy than GeSn. However, predictive accuracy is limited by two factors: (i) VCA cannot adequately describe alloy disorder in group-IV semiconductors [19], and (ii) conventional DFT tends to underestimate bandgaps [20]. Therefore, the Pb crossover concentration reported by Liu et al. [20] likely requires further correction.

Like GeSn, GePb has major drawbacks: the solid solubility of Pb in Ge is very low [21-24], and the lattice mismatch between each other is very large, which results in a very low substitutional Pb concentration in the GePb alloy. So, reducing the need for Pb to create a direct bandgap is critical to the crystal growth and device application of GePb alloy. Besides increasing Pb concentration, applying external strains to GePb also could create a direct bandgap, like strained Ge and GeSn alloys which have supported to change from indirect to direct bandgaps by applying suitable strains [25-26]. The combination of these two methods might be a more efficient approach to reduce the reliance on Pb in direct-bandgap GePb.

In this work, a GeSiPb/GePb/GeSiPb Barrier-Well-Barrier structure heterostructure is proposed and analyzed. The widths of the well and barrier are taken as 16 nm and 72 nm respectively. The layer-by-layer heterostructure is designed using the Silvaco TCAD simulation platform, introducing GePb as a novel material component. The energy-band profile of the proposed structure is investigated through simulation, revealing that the heterostructure exhibits a type-II band alignment under compressive strain. Analytical and simulated results for the band alignment and band offsets are evaluated and compared. The GeSiPb/GePb/GeSiPb heterostructure enables spatial confinement of electrons and holes, enhancing the overlap of electron–hole wave functions and facilitating direct transitions in the $Ge_{0.98}Pb_{0.02}$ well region. Additionally, optical gain and absorption characteristics are computed for GePb-based alloys grown on SiGePb barriers, further demonstrating the potential of this material system for optoelectronic applications. Our proposed design discusses that a Pb concentration of 2 % within the well region is adequate to attain direct bandgap characteristics with the application of compressive strain in the heterostructure, whereas previous research indicates approximately 3 % Pb crossover for direct bandgap in bulk GePb.

Within the KP framework, the heterostructure band edges are obtained from the carriers' energy eigenvalues and eigen functions, providing direct insight into the fundamental nature of the band alignment. This methodology allows for the quantitative prediction and validation of the indirect-to-direct bandgap crossover and the emergence of Type-II alignment, even at relatively low Pb concentrations [27].

Furthermore, the optical behavior of these alloys is analyzed, supported by systematically organized computational results and key observations. The discussion concludes with a summary of current knowledge and highlights future research prospects in the field.

2. Methodology

The heterostructure is developed forming a GePb/GeSiPb barrier/well/barrier model. In this study, supercell models are employed to simulate $Ge_{1-p}Pb_p$ alloys, with the proposed model illustrated in Fig. 1. $Ge_{1-p}Pb_p$ with different Pb concentration can be simulated by changing the number of Pb atoms and the size of models, (111)-biaxial strains are parallel to (111)-orientation.

The proposed model serves as a visual representation of the system under investigation, offering insights into the behavior and properties of Ge1-pPbp alloys. A Virtual Substrate (VS) [28],

typically consisting of a standard substrate (like silicon) and a relaxed buffer layer on top is used in heterostructures to provide a compatible lattice constant for growing layers of different materials on a single Si Substrate. Through these simulations, researchers can analyze the effects of Pb concentration on the overall characteristics and behavior of the alloy.

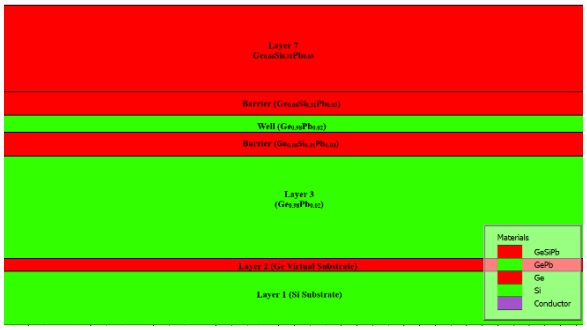

Fig. 1. Simulated Ge_1-pPb_p/$Ge_{1-x-y}Si_xPb_y$ heterostructure.

3. Calculation of Absorption Coefficient

The absorption coefficient, α, is a property of a material which defines the amount of light absorbed by it. The inverse of the absorption coefficient, α^{-1}, is the average distance traveled by a photon before it gets absorbed. The inverse of the absorption coefficient also is the distance at which its intensity of light is reduced to a value 1/e (~36 %) of its original intensity [Basu 2003].

The absorption coefficient for direct transition as a function of photon energy ħω can be written as [29]:

$$\alpha\left(\hbar\omega\right) = \frac{q^2(2m_r)^{3/2}}{2\pi\varepsilon_0 c\eta m_0^2\hbar^2}\frac{(\hbar\omega - E_g)^{3/2}}{\hbar\omega}\langle|p_{cv}^2|\rangle, \qquad (1)$$

where q is the electronic charge = 1.6×10^{-19} C, m_r is the reduced mass and it is expressed as, $m_r^{-1} = m_e^{-1} + m_h^{-1}$, m_e is the reduced mass for electrons, m_h is the reduced mass for holes, η is the refractive index, ε_0 is the permittivity of free space = 8.854×10^{-12} F/m, c is the velocity of light in free space = 3×10^8 m/s, m_0 is the free electron rest mass = 9.11×10^{-31} Kg, h is the Planck's constant = 4.135×10^{-15} eV-s, ħ = h/2π = 1.054×10^{-34} J-s, E_g is the bandgap energy,

$\langle|p_{cv}^2|\rangle$ is the average of the square matrix element for transitions between Bloch states in the valence and conduction bands. The expression for $\langle|p_{cv}^2|\rangle$ for unpolarized light is given by [30]:

$$\langle|p_{cv}^2|\rangle = \frac{m_0^2 E_g(E_g+\Delta)}{3m_e(E_g+{}^{2\Delta}/_3)} \qquad (2)$$

To calculate all parameters, the composition of each material has also been considered using Vegard's Law. By using the absorption coefficient equation, a plot of the absorption coefficient as a function of photon energy (ħω) is obtained.

4. Calculation of Gain

If electrons are injected into the conduction band and holes into the valence band (as happens for light emitting devices) the electron-hole pairs may recombine and emit more photons than can be absorbed. Thus, one must consider the emission coefficient minus the absorption coefficient. This term is called the gain of a material.

For the simple parabolic bands, the gain g(ħω) is given by the generalization of our result for the absorption coefficient (gain = emission coefficient-absorption coefficient).

$$g(\omega) = \alpha\,(\hbar\omega)\,[f^e(E^e) - (1 - f^h(E^h))] \qquad (3)$$

The term in the square brackets arises since the emission of photons in proportional to $f^e.\ f^h$, while the absorption process is proportional to $(1\text{-}f^e).(1\text{-}f^h)$. The difference of these terms appear in the above equation.

5.Results and Performance Analysis

In the present work, firstly the band edges and band offsets for the material $Ge_{1-p}Pb_p/Ge_{1-x-y}Si_xPb_y$ have been calculated. It is found the GePb becomes the direct band gap material for a wide range of concentration and band alignment is type II, with both the valence band and conduction band edges localized in the GePb layer. Here the concentration for Pb is chosen to its maximum limit (= 3 %). The parameters used for our calculation are listed in the Table 1. The concentration of Pb is so chosen that the barrier-well-barrier heterostructure $Ge_{1-p}Pb_p/Ge_{1-x-y}Si_xPb_y$ has become direct band structure.

Table 1. Different Parameters for Ge, Si and Pb.

Material Specifications	Ge	Si	Pb
Electron Affinity (eV)	4.0 [36]	4.05 [36]	0.356 [36]
$E_{g,\Gamma}$ (eV)	0.7985 [31]	4.185 [31]	0.513 [16]
$E_{g,L}$ (eV)	0.664 [31]	1.65 [31]	-
$\Delta E_{v,av}$ (eV)	0 [31]	-0.48 [31]	-
μ_n $cm^2s^{-1}V^{-1}$	3900 [35]	1400 [35]	Not Known
μ_p $cm^2s^{-1}V^{-1}$	1900 [35]	450 [35]	Not Known
τ (S)	10^{-3} [34]	2.5×10^{-3} [34]	Not Known
E_g (eV)	0.66 [35]	1.12 [34]	-
Dielectric constant ϵ_r	16.2 [31]	11.9 [31]	-

In the proposed heterostructure model, the Pb concentration is intentionally varied from 3 % in the barrier (GeSiPb) and 2 % in the well (GePb). This compositional tuning plays a crucial role in achieving the desired direct bandgap with Type-II band alignment while maintaining good lattice compatibility and strain balance between the layers. The difference in Pb concentration (1 %) between the barrier and well establishes a potential well (quantum confinement potential), thereby trapping carriers within discrete energy states in the well. Also, the Pb concentration variations in barrier and well region creates narrow bandgap in the well region and slightly wider bandgap in the barrier region.

In this study, the alloy material Pb has been introduced in the SiGe Heterostructure. $Ge_{1-x}Si_x$ alloy with an α-Pb composition more than the critical value for the indirect-to-direct bandgap transition for the QW material is considered in our calculation. In addition to this, different doping levels are considered in accordance with the regions of emitter, base and collector. The energy-band profile of the proposed heterostructure has been studied using Silvaco TCAD Tool shown in Fig. 2. From the energy-band profile observed from the Silvaco-TCAD, the type-II band alignment has been seen. The electrons and holes can be spatially confined in the $Ge_{0.98}Pb_{0.02}$ well in the heterostructure $Ge_{1-p}Pb_p/Ge_{1-x-y}Si_xPb_y$. This leads to improved electron–hole spatial wavefunction overlaps for the direct transitions. In the $Ge_{0.98}Pb_{0.02}$ well region, the compressive strain is in the percentage of 0.50 % which has been considered during layer-by-layer growth in Silvaco TCAD simulator. The effect on the different loss mechanisms like free carrier absorption, spontaneous recombination and Auger recombination become vital as barrier-well-barrier heterostructure structure and are considered during the calculation of optical absorption and optical gain. The electrical parameters including electron mobility, hole mobility, lifetime of electron & holes, electron affinity, energy gap and permittivity are calculated by using Vegard's Law.

From the calculation of type-II band alignment, the conduction band offset has been evaluated. A comparison of the type-II conduction band offset with respect to theoretical and simulated value is outlined below.

5.1. Abbreviations and Acronyms

$E_{g,\Gamma}$ is the bandgap of conduction band edge at the Γ point of the Brillouin zone [31].

$E_{g,L}$ is the bandgap of conduction band edge at the L point of the Brillouin zone [31].

$\Delta E_{v,av}$ is the offset average of the three top valence bands and $\Delta E_{v,av}(x,y) = 0.69 \times y - 0.48 \times x$ [32, 37].

E_g is the bandgap at room temperature [36].

μ_n is the electron mobility, μ_p is the hole mobility [34].

τ is the minority carrier lifetime [34].

Expression of Vegard's law (linear interpolation) [31] for $Ge_{1-x-y}Si_xPb_y$:

$$[a_{Ge_{1-x-y}Si_xPb_y} = x \times a_{Si} + y \times a_{Pb} + (1-x-y) \times a_{Ge}]$$

Expression of Vegard's law for $Ge_{1-p}Pb_p$:

$$[a_{Ge_{1-p}Pb_p} = (1-p) \times a_{Ge} + p \times a_{Pb}]$$
$$(x = 0.31,\ y = 0.03\ \&\ p = 0.02)$$

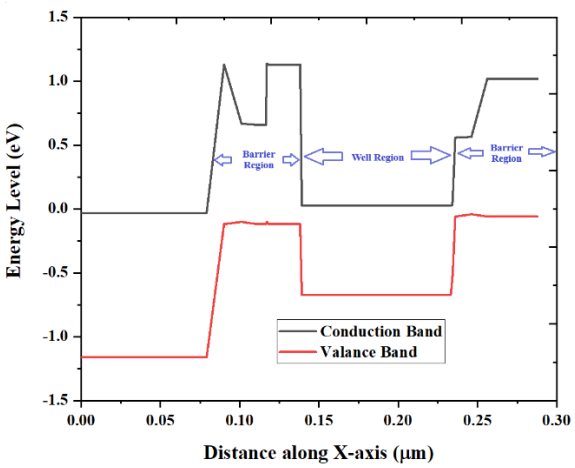

Fig. 2. Energy band profile of $Ge_{1-p}Pb_p/Ge_{1-x-y}Si_xPb_y$ structure.

All the parameters of the new materials are calculated using this mathematical expression and are included in Silvaco coding.

Table 2. Calculated Values of Parameters for $Ge_{1-p}Pb_p$ and $Ge_{1-x-y}Si_xPb_y$

Material Specifications	**$Ge_{1-p}Pb_p$ p = 0.02**	**$Ge_{1-x-y}Si_xPb_y$ x = 0.31, y = 0.03**
Electron Affinity (eV)	3.92712	3.9061
$E_{g,\Gamma}$ (eV)	0.7927	1.83975
$E_{g,L}$ (eV)	0.651	0.9497
$\Delta E_{v,av}$ (eV)	0	-0.79
μ_n $cm^2s^{-1}V^{-1}$	3822	3008
μ_p $cm^2s^{-1}V^{-1}$	1862	1393.5
τ (S)	0.00098	0.001435
E_g (eV)	0.6468	0.7828
Dielectric constant ϵ_r	15.876	14.381

This statement clarifies that all characteristics depending on linearity, notably carrier lifetimes and

mobilities, have been assessed utilizing Vegard's law [31] through linear interpolation. This ensures that the compositional dependence of these parameters follows an established and physically accepted averaging scheme for alloy systems. Furthermore, to address any deviations that may arise due to lattice mismatch or compositional grading, strain-balanced methodology [31] has been utilized. This approach ensures that the structural and electronic properties remain consistent across the heterostructure, thereby maintaining linearity in the interpolated parameters and preventing physically inconsistent distortions in the band structure.

Table 3. Simulated Values of Conduction Band and Valance Band Edges of Type-II $Ge_{1-p}Pb_p/Ge_{1-x-y}Si_xPb_y$ Structures.

Barrier-Well-Barrier QW Heterostructure Specification (eV)	**$Ge_{1-p}Pb_p/Ge_{1-x-y}Si_xPb_y$**
Simulated E_{C1}	1.1045
Simulated E_{C2}	0.0269
Simulated E_{V1}	-0.12
Simulated E_{V2}	-0.6253

Table 4. Simulated and Theoretical Values of Conduction Band Offset of Type-II $Ge_{1-p}Pb_p/Ge_{1-x-y}Si_xPb_y$ Structures.

Barrier-Well-Barrier QW Heterostructure Specification	**$Ge_{1-p}Pb_p$ /$Ge_{1-x-y}Si_xPb_y$**
Simulated Conduction Band Offset (E_{C1} - E_{C2}) (eV)	1.0776
Theoretical Conduction Band Offset (E_{C1} - E_{C2}) (eV)	1.0854 [38]

Here, $E_{C1} > E_{C2}$ and $E_{V1} > E_{V2}$ for $Ge_{1-p}Pb_p/Ge_{1-x-y}Si_xPb_y$ structures. So, the designed heterostructure is a Type-II System.

5.2. Nobility & Uniqueness

The proposed GePb/GeSiPb heterostructure study exhibits a desirable Direct Bandgap with Type-II band alignment at a Pb concentration of 2 % in the well region. This result is particularly noteworthy because most reported works [6, 20, 33] have required higher Pb concentrations (for example, 5–8 %) to achieve a desirable alignment. Lower Pb concentration in the well (2 %) and a slightly higher Pb in the barrier (3 %) also recommends the lattice constants of the two regions remain more compatible, thereby reduces the elastic strain and structural defects. This band gap shift is mainly due to the lattice parameter difference between GePb and tensile strained Ge. The Type-II direct bandgap behavior makes the proposed heterostructure a promising candidate in the domain of photonics.

In the next section, a study is carried out to investigate achievement optical gain in group IV semiconductors with the incorporation of alloying Pb in $Ge_{1-x}Si_x$ semiconductor.

The study includes the observation of the variation of absorption coefficients of the proposed structure with the variation of photon energy plotted in Fig. 3. These results lead to the observation of the change in optical gain vs. photon energy plotted in Fig. 4 and the amount of gain is obtained from the study is most desirable for high frequency communication windows. In addition, aiming to the lighting efficiency of $Ge_{1-p}Pb_p$, the optical gain of strained $Ge_{1-p}Pb_p/Ge_{1-x-y}Si_xPb_y$ is evaluated and compared. The photon range obtained from the study concludes that proposed model can be used in high frequency telecommunication range with appreciable optical gain. The optical gain of the proposed model is compared with the relevant experimental value. The comparison is shown in Fig. 5. The comparison of the peak value of the optical gain is shown in Table 5. From the comparison it can be seen that though the values match moderately but it can be concluded the higher value of the optical gain can be obtained at high frequencies.

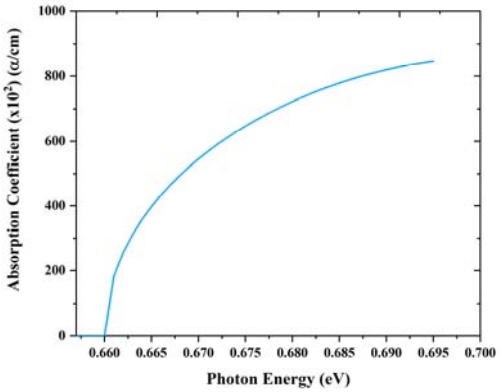

Fig. 3. Variation of the absorption coefficient with different photon energy for $Ge_{1-p}Pb_p/Ge_{1-x-y}Si_xPb_y$. Heterostructure.

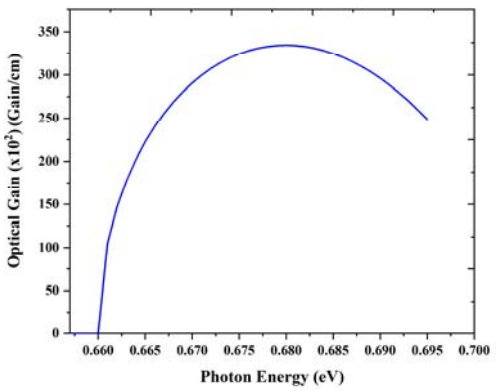

Fig. 4. Variation of the gain coefficient with different photon energy for $Ge_{1-p}Pb_p/Ge_{1-x-y}Si_xPb_y$

Table 5. Comparison of Peak Values of Optical Gain with Simulated Structure and Reference Structure of unstrained $Ge_{1-p}Pb_p$ with a concentration of 3 % Pb as a function of Photon Energy.

Parameter Specifications (gain/cm)	Simulation work	Reference Work [16]
Optical Gain (max)	334.54×10^2 (Photon Energy = 0.68 eV)	203.323 (Photon Energy = 0.562 eV)

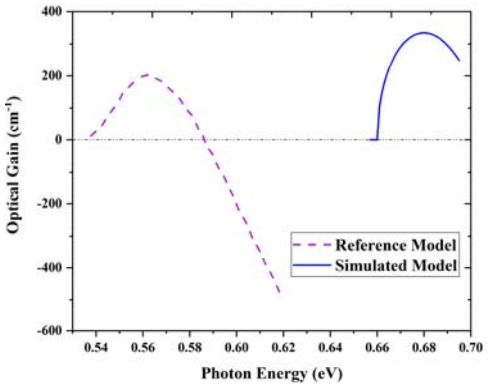

Fig. 5. Comparison of Variation of the Gain coefficient with different Photon Energy for a Reference Structure [16] and Proposed Model.

In Fig. 5, a comparative study optical gain of the proposed model is observed with a reference model. The reference model indicates approximately 3 % Pb concentration in bulk GePb whereas a Pb concentration of 2 % is utilized for operating the proposed model (well region). Thus, the proposed device has a higher range of photon energy thereby a wider bandgap. The difference of photon energies in the proposed model and the reference model is mainly due to the difference in the concentration of Pb. From the proposed device, the desirable Direct Bandgap with Type-II band alignment is achieved with a 2 % concentration of Pb, lower than the concentration value of bulk GePb. The wider bandgap is particularly important for allowing devices that use them to operate at much higher temperatures. The high temperature tolerance also means that these devices can be operated at much higher power levels. Also, the composition of Ge is different in barrier and well regions. Additionally, in our simulations, parameters such as band offsets, effective masses, and recombination coefficients were computed using Vegard's law and included strain effects, which are absent in the reference structure. These simulation considerations further contribute to the observed energy shift.

6. Conclusion

This work uses TCAD simulations to analyze a $Ge_{0.66}Si_{0.31}Pb_{0.03}/Ge_{0.98}Pb_{0.02}/Ge_{0.66}Si_{0.31}Pb_{0.03}$ barrier–well–barrier heterostructure, focusing on its band alignment, absorption behavior, and optical gain characteristics for prospective optoelectronic applications. Introducing 3 % Pb into the GeSiPb barrier layers and 2 % Pb into the GePb well produces an alloy system with reduced lattice mismatch and enhanced flexibility in tuning electronic states. The band offset calculations show a clear Type-II staggered alignment under compressive strain, with conduction- and valence-band discontinuities that promote spatial separation of electrons and holes. These findings are predictive in nature, being derived from Vegard's law–based parameter interpolation and TCAD material models; therefore, experimental validation of gain and material quality remains essential. The extracted absorption coefficients further highlight how integrating a quantum well enhances the absorption of lower-energy photons. Overall, the results indicate that Pb inclusion in group-IV alloys offers a promising route for bandgap engineering, yielding electronic and optical properties not accessible in conventional Ge-based heterostructures.

A layer-by-layer barrier-well-barrier structure of $Ge_{0.66}Si_{0.31}Pb_{0.03}/Ge_{0.98}Pb_{0.02}/Ge_{0.66}Si_{0.31}Pb_{0.03}$ is formed using Si Substrate and Ge buffer (Virtual substrate). The schematic structure of Transistor Laser using $Ge_{1-p}Pb_p/Ge_{1-x-y}Si_xPb_y$ simulated by Silvaco TCAD is shown in Fig. 1. Layer 1, with a width of 50 nm, holds the Si substate over which a Ge buffer (VS) (layer 2) is developed with a width of 15 nm. Layer 3 (95 nm) is formed with GePb layer with a concentration of 2 % Pb over the layer 2. The barrier-well-barrier model is created with layer 4, layer 5 and layer 6 respectively. The width of the total active layer is 60 nm. The barrier width is considered as 22 nm and well width is considered as 16 nm. These three layers holding the barrier-well-barrier model serve as the active region of the device having a doping (p-type) level of 10^{17} atoms per cm^3. The topmost layer (Layer 7) is formed by $Ge_{1-x-y}Si_xPb_y$ (x = 0.31 & y = 0.03) with a doping level (n-type) of 10^{20} atoms per cm^3.

The current research primarily focuses on investigating the characteristics of the bandgap, band offsets, and quantum confinement effects within the structure. The study is in scope to advance further by incorporating bias-dependent simulations that include free-carrier and Auger loss mechanisms, along with sensitivity analyses to evaluate dynamic carrier transport, current–voltage characteristics, and optical response of the structure under realistic operating conditions ultimately yielding a more comprehensive heterostructure model utilizing Group IV elements.

Acknowledgements

The author wishes to express their sincere gratitude to V Chakraborty, S. Dey, A. Saha and R. S. Dhar for their invaluable contributions to this research. Specifically, I thank V. Chakraborty & S. Dey for their expertise in the domain of bandgap engineering with

Gr-IV based materials and its implementation in optics and A. Saha & R. S. Dhar for their crucial role in Silvaco TCAD simulation and device modelling. Their collaborative spirit and dedication were essential to the completion and success of this work.

References

[1]. Q. M. Thai, J. Chretien, M. Bertrand, L. Casiez, et al., GeSn optical gain and lasing characteristics modelling, *Physical Review B*, Vol. 102, Issue 15, 2020, 155203.

[2]. J. Liu, Monolithically integrated Ge-on-Si active photonics, *Photonics*, Vol. 1, Issue 3, 2014, pp. 162-197.

[3]. W. Huang, B. Cheng, C. Xue, C. Li, Comparative studies of clustering effect, electronic and optical properties for GePb and GeSn alloys with low Pb and Sn concentration, *Physica B: Condensed Matter*, Vol. 443, 2014, pp. 43-48.

[4]. N. S. Ghosh, B. Mukhopadhyay, G. Sen, Performance enhancement of GeSn transistor laser with symmetric and asymmetric multiple quantum well in the base, *Semiconductors*, Vol. 54, Issue 1, 2020, pp. 77-84.

[5]. S. Ghosh, G. Sun, T. A. Morgan, G. T. Forcherio, et al., Dark current analysis on GeSn p-i-n photodetectors, *Sensors*, Vol. 23, Issue 17, 2023, 7531.

[6]. X. Liu, J. Zheng, Q. Huang, Y. Pang, et al., Growth and characterization of GePb/Ge multiple quantum wells, *Journal of Alloys and Compounds*, Vol. 934, 2023, 167954.

[7]. W. Hu, X. Xie, Q. Xu, S. Huang, et al., Research progress on preparation technology and application of near-infrared silicon-based materials, *Proceedings of SPIE*, Vol. 12166, 2022, 121661A.

[8]. N. Shaw, B. Mukhopadhyay, Performance assessment of a dielectrically modulated SiGe-pocket DG TFET-based biosensor, in *Proceedings of the IEEE International Conference of Electron Devices Society Kolkata Chapter (EDKCON'22)*, 2022, pp. 217-220.

[9]. P. K. Basu, B. Mukhopadhyay, R. Basu, Semiconductor Nanophotonics, *Oxford Univ. Press*, 2022.

[10]. T. T. McCarthy, A. M. McMinn, X. Liu, R. Hossain, et al., Molecular beam epitaxy growth and characterization of GePb alloys, *Journal of Vacuum Science & Technology B*, Vol. 42, Issue 3, 2024, 031201.

[11]. P. K. Basu, Theory of Optical Processes in Semiconductors: Bulk and Microstructures, *Oxford Univ. Press*, Oxford, UK, 2003.

[12]. G. T. Reed, A. P. Knights, Silicon Photonics: An Introduction, *Wiley*, 2004.

[13]. M. J. Deen, P. K. Basu, Silicon Photonics: Fundamentals and Devices, *Wiley*, Chichester, 2012.

[14]. N. Izhaky, M. T. Morse, S. Koehl, O. Cohen, et al., Development of CMOS-compatible integrated silicon photonics devices, *IEEE Journal of Selected Topics in Quantum Electronics*, Vol. 12, Issue 6, 2006, pp. 1688-1698.

[15]. R. A. Soref, L. Friedman, Direct-gap Ge/SnSiGe heterostructures, *Superlattices and Microstructures*, Vol. 14, Issue 2-3, 1993, pp. 189-193.

[16]. W. Huang, B. Cheng, C. Xue, H. Yang, The band structure and optical gain of a new IV-group alloy GePb: A first-principles calculation, *Journal of Alloys and Compounds*, Vol. 701, 2017, pp. 816-821.

[17]. B. Bouhafs, F. Benkabou, M. Ferhat, B. Khelifa, et al., Energy band structure calculation of Ge_xSn_{1-x} and Si_xSn_{1-x} alloys, *Infrared Physics & Technology*, Vol. 36, Issue 6, 1995, pp. 967-972.

[18]. X. Liu, J. Zheng, L. Zhou, Z. Liu, et al., Growth of single crystalline GePb film on Ge substrate by magnetron sputtering epitaxy, *Journal of Alloys and Compounds*, Vol. 785, 2019, pp. 228-231.

[19]. S. Xia, J. Yu, J. Wang, W. Huang, et al., A first-principle study on the band structure of GePb alloys, *Semiconductor Science and Technology*, Vol. 39, Issue 12, 2024, 125020.

[20]. X. Liu, J. Zheng, X. Li, Z. Liu, et al., Study of GePb photodetectors for shortwave infrared detection, *Optics Express*, Vol. 27, Issue 13, 2019, pp. 18038-18045.

[21]. L. Von Szentpály, Atom-based thermochemistry: Crystal atomization and sublimation enthalpies in linear relationships to molecular atomization enthalpy, *Journal of the American Chemical Society*, Vol. 130, Issue 18, 2008, pp. 5962-5973.

[22]. A. Ciccioli, G. Gigli, G. Meloni, E. Testani, The dissociation energy of the new diatomic molecules SiPb and GePb, *The Journal of Chemical Physics*, Vol. 127, Issue 5, 2007, 054303.

[23]. H. Johll, M. Samuel, R. Y. Koo, H. C. Kang, et al., Influence of hydrogen surface passivation on Sn segregation, aggregation, and distribution in GeSn/Ge(001) materials, *Journal of Applied Physics*, Vol. 117, Issue 20, 2015, 205305.

[24]. D. Scopece, F. Montalenti, M. Bollani, D. Chrastina, et al., Straining Ge bulk and nanomembranes for optoelectronic applications: a systematic numerical analysis, *Semiconductor Science and Technology*, Vol. 29, Issue 9, 2014, 095012.

[25]. M. J. Süess, R. Geiger, R. A. Minamisawa, G. Schiefler, et al., Analysis of enhanced light emission from highly strained germanium microbridges, *Nature Photonics*, Vol. 7, Issue 6, 2013, pp. 466-472.

[26]. V. R. D'Costa, W. Wang, Q. Zhou, E. S. Tok, et al., Above-bandgap optical properties of biaxially strained GeSn alloys grown by molecular beam epitaxy, *Applied Physics Letters*, Vol. 104, Issue 2, 2014, 022111.

[27]. M. Cardona, F. H. Pollak, Energy-band structure of germanium and silicon: The k·p method, *Physical Review*, Vol. 142, Issue 2, 1966, pp. 530-543.

[28]. A. K. Pandey, R. Basu, Characteristics of GeSn-based multiple quantum well heterojunction phototransistors: a simulation-based analysis, *IET Optoelectronics*, Vol. 12, Issue 3, 2018, pp. 144-149.

[29]. V. Chakraborty, B. Mukhopadhyay, P. K. Basu, Effect of different loss mechanisms in SiGeSn based mid-infrared laser, *Semiconductors*, Vol. 49, Issue 6, 2015, pp. 836-842.

[30]. V. Chakraborty, S. Dey, R. Basu, B. Mukhopadhyay, et al., Current gain and external quantum efficiency modeling of GeSn based direct bandgap multiple quantum well heterojunction phototransistor, *Optical and Quantum Electronics*, Vol. 49, Issue 3, 2017, 100.

[31]. G. Chang, S. Chang, S. L. Chuang, Strain-balanced Ge_zSn_{1-z}-$Si_xGe_ySn_{1-x-y}$ multiple-quantum-well lasers, *IEEE Journal of Quantum Electronics*, Vol. 46, Issue 12, 2010, pp. 1813-1820.

[32]. S. Dey, B. Mukhopadhyay, G. Sen, P. Basu, Type II band alignment in $Ge_{1-x-y}Si_xSn_y/Ge_{1-\alpha-\beta}Si_\alpha Sn_\beta$ heterojunctions, *Solid State Communications*, Vol. 270, 2018, pp. 155-159.

[33]. X. Liu, J. Zheng, Q. Huang, J. Cui, et al., Investigation of temperature and H_2 on GePb/Ge multiple quantum well growth, *Journal of Physics D: Applied Physics*, Vol. 57, Issue 24, 2024, 245108.
[34]. S. L. Chuang, Physics of Optoelectronic Devices, *Wiley*, 1995.
[35]. M. Safi, A. Aissat, H. Guesmi, J. P. Vilcot, SiGe quantum wells implementation in Si based nanowires for solar cells applications, *Digest Journal of Nanomaterials and Biostructures*, Vol. 18, Issue 1, 2023, pp. 327-342.
[36]. D. Bresteau, C. Drag, C. Blondel, Electron affinity of lead, *Journal of Physics B: Atomic, Molecular and Optical Physics*, Vol. 52, Issue 6, 2019, 065001.
[37]. J. Menéndez, J. Kouvetakis, Type-I $Ge/Ge_{1-x-y}Si_xSn_y$ strained-layer heterostructures with a direct Ge bandgap, *Applied Physics Letters*, Vol. 85, Issue 7, 2004, pp. 1175-1177.
[38]. S. Dey, V. Chakraborty, B. Mukhopadhyay, G. Sen, Modeling of tunneling current density of GeC based double barrier multiple quantum well resonant tunneling diode, *Journal of Semiconductors*, Vol. 39, Issue 10, 2018, 104003.